Modelling the radiation efficiency of orthotropic cross-laminated timber plates with simply-supported boundaries

Andrea Santoni[a,*], Stefan Schoenwald[b], Patrizio Fausti[a], Hans-Martin Tröbs[b]

[a]*Engineering Department, University of Ferrara, via G. Saragat 1, 44122 Ferrara, Italy*
[b]*Laboratory for Acoustics and Noise Control, Empa - Swiss Federal Laboratories for Material Science and Technology, Ueberlandstrasse 129, CH-8600 Dübendorf, Switzerland*

Abstract

In this paper two prediction models to evaluate the radiation efficiency of orthotropic plates, developed with different approaches, are presented. A sound radiation model, based on an analytical/modal approach, is developed for a thin orthotropic plate, with the principal directions aligned with the edges. The model allows to consider the contribution of each mode, either resonant or non-resonant, as well as the influence of fluid loading on the plate dynamic response and on sound radiation. Moreover, a statistical model to evaluate the average radiation efficiency, based on a non-modal approach, which only considers the contribution of resonant modes, is presented. These two models have been used in order to predict the radiation efficiency of orthotropic cross-laminated timber (CLT) plates. CLT is an engineered wood material constituted by an odd number of lumber beams glued together, which have become very popular in the last twenty years in the building construction market. Due to their layered structure, CLT plates might exhibit a highly orthotropic behaviour. Both prediction models are validated by comparing the simulated results with the experimental radiation efficiency, obtained by means of vibro-acoustic measurements on three CLT plates. Finally, the influence of fluid loading on sound power radiated by CLT plates is investigated.

Keywords: radiation efficiency, orthotropic plate, cross-laminated timber, fluid-loading influence

1. Introduction

Noise reduction is nowadays a main concern as much in the automotive or aerospace industry as in building construction and in many other fields. In order to design structures that provide good sound insulation it is fundamental to characterise how the vibrating elements radiate sound. Sound radiation has been the object of an increasing interest during the last half century and the physics behind this mechanism is well known. However, from an engineering point of view, the computation of the sound power radiated by a vibrating surface is still a highly demanding task compared to pure vibrational problems. In order to provide reliable alternatives to finite elements (FE) and boundary elements methods (BEM), which usually require a considerable

*Corresponding author
Email address: andrea.santoni@unife.it (Andrea Santoni)

Article accepted in Applied Acoustics *23 August 2018*

computational effort, many formulations to predict the radiated sound power have been proposed by several authors. These prediction models provide approximated results with wide-ranging levels of accuracy. They have been developed by using different approaches and under different basic assumptions, upon which depends their suitability for each specific problem. Based on a *non–modal approach*, the modal-average radiation efficiency due to the contribution of the resonant vibrational field can be evaluated [1]. On the other hand, using a *modal approach* the radiation efficiency is approximated by taking into account all the in-vacuo single modes within the frequency range [2]. In order to consider the influence of cross-modal coupling, different *analytical formulations* have been developed using either the far field [3], or the near-field approach [4]; the latter also takes into account the fluid loading effect. An extensive and more detailed bibliographic analysis of the prediction models to compute sound radiation was presented by Atalla and Nicolas in 1994 [5]. Later in the same decade Nelisse [6] proposed a generalized model for the acoustic radiation from baffled and unbaffled homogeneous plates, with arbitrary boundary conditions. The same approach was also used by Foin to develop a tool to predict the acoustic and structural vibration response of sandwich plates [7]. More recently Mejdi and Atalla presented a semi-analytical model to numerically investigate the vibro-acoustic response of stiffened plates [8], while Legault analysed orthogonally ribbed plates by means of a periodic theory [9]. Rhazi and Atalla used simple and quick tools, such as statistical energy analysis and the transfer matrix method, to estimate the vibro-acoustic response of mechanically-excited multilayer structures [10]. Davy developed a two dimensional strip analytic approximation to compute the forced radiation efficiency of acoustically excited finite size panels [11]. Davy also presented an approximation method to calculate both the real and the imaginary part of the single-side specific forced radiation impedance of a rectangular panel [12]. The possibility to consider both the resonant and non resonant contribution, in the case of an acoustically excited plate, and the near-field contribution in the case of mechanical point excitation, was also introduced by Davy in a recently published paper [13].

Two models are presented in this paper; they have been implemented in order to estimate the radiation efficiency of mechanically excited orthotropic panels, such as cross-laminated timber plates used in buildings. Cross-laminated timber solid wood panels, commonly known as CLT, consist of an odd number of layers of lumber beams glued together, alternating the fibres orientation of adjoining plies orthogonally. This engineered wood material has gained a growing success in the construction market over the last two decades, especially in Europe and North America. In fact in recent years, CLT has also attracted the interest of acousticians and researchers who have carried out experimental investigations on these structures [14–18]. Nowadays, CLT structures represent a valuable alternative to traditional construction materials. They provide good structural stability, fulfil the safety requirements and allow to reduce construction time, since they can be completely prefabricated and then assembled at the construction site. The drawback of this construction technology is arguably the poor sound insulation provided by CLT panels, due to their low density combined with a relatively high stiffness. During the design process it is necessary to acoustically optimize the CLT elements in order to improve the sound insulation performace and meet the acoustic requirements for buildings [19]. Due to their layered sub-structure and the properties of the wood material, CLT plates generally exhibit an orthotropic behaviour [20, 21], which means that they have different elastic properties along mutually perpendicular directions. CLT panels can be investigated as 3D orthotropic plates. This approach, however, would involve a rather tedious and complex analysis with nine independent elastic constants to be known: i.e. three elastic moduli and three Poisson's ratios associated with the the principal directions and three shear moduli. In order to define more usable models, the thin plate theory is here adopted, since it greatly simplifies the problem, describing the orthotropic constitutive relationship by means of only five independent constants. However, in order to take into account the influence of rotatory inertia and shear deformation, which are neglected in the thin plate theory but might be significant especially in the high frequency range, the CLT panels are described by means of apparent frequency-dependent elastic properties, as further discussed below.

In the next section the numerical models to predict the radiation efficiency of orthotropic plates are introduced. At first, an analytical formulation for a thin orthotropic plate is derived, by following the general approach, based on a variational formulation, proposed by Nelisse [6]. Then a simplified modal-average approach to compute the orthotropic radiation efficiency, based on more restrictive assumptions, is described. Both models have been validated with the experimental radiation efficiency evaluated for three different CLT plates, as described in section 3. The main results are presented and discussed in section 4.

2. Prediction models for an orthotropic plate

The radiation efficiency σ is defined as the ratio between the sound power W_{rad} actually radiated by a vibrating elastic structure and the sound power that would theoretically be radiated by a rigid piston of equal surface area S vibrating with the same mean square velocity $\left\langle v^2 \right\rangle_{s,t}$, where the subscript $_{s,t}$ indicates time and spatial average, multiplied by the characteristic air impedance $Z_0 = \rho_0 c_0$:

$$\sigma = \frac{W_{rad}}{\rho_0 c_0 S \left\langle v^2 \right\rangle_{s,t}}. \tag{1}$$

where ρ_0 is the density of the fluid medium and c_0 the speed of sound within the fluid. This acoustic descriptor, characterising the capability of a vibrating structure to transfer the vibrational energy to the surrounding fluid as sound energy, represents important input data, required in the greatest part of building acoustics prediction models [22–26]. In this section two models to evaluate the radiation efficiency of an orthotropic rectangular plate are presented. They are based on different assumptions and developed following distinct approaches. An analytical/modal-based approach is derived, either considering or neglecting the influence of fluid loading. Then a modal-average model, which may be useful within the statistical energy analysis (SEA) framework, is presented.

Both models assume the validity of thin plate theory. However, as the frequency increases and the structural wavelength approaches the panel thickness, rotational inertia and shear deformation effects start to have a significant influence on the plate dynamics. For this reason, apparent frequency-dependent stiffness properties have been introduced in order to adopt low-order theories while considering several effects which take part in the flexural motion, such as shear deformation, rotatory inertia, viscoelasticity and the layered substructure. The possibility to adopt such a homognenisation approach, commonly used to investigate sandwich structures [27–29], also to CLT panels has already been successfully investigated and discussed by other authors in previous studies [20, 30].

2.1. Modal based radiation and fluid-loading

Let us consider a rectangular thin orthotropic plate, with the principal axes aligned with the edges, lying in the $x - y$ plane and inserted in a coplanar rigid baffle, as shown in Figure 1.

Published article available online: https://doi.org/10.1016/j.apacoust.2018.08.022

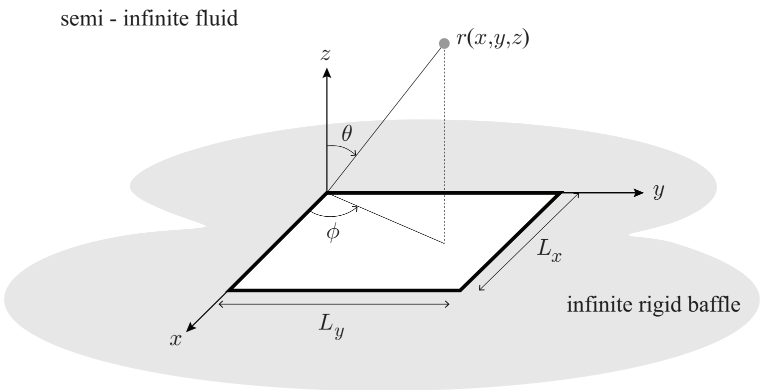

Figure 1: Elastic thin orthotropic plate inserted in a infinite rigid baffle, radiating sound energy in a semi-infinite fluid domain $z > 0$.

The equation of motion of such a thin orthotropic plate, undergoing free flexural vibrations, is governed by the fourth-order in space and second-order in time differential equation:

$$D_x \frac{\partial^4 w}{\partial x^4} + 2B \frac{\partial^4 w}{\partial x^2 \partial y^2} + D_y \frac{\partial^4 w}{\partial y^4} = \rho h \frac{\partial^2 w}{\partial t^2}. \tag{2}$$

The bending stiffness along the principal directions, D_x and D_y, and the effective torsional stiffness B, are a function of elastic and in-plane shear moduli E_x, E_y and G_{xy}:

$$D_x = \frac{E_x h^3}{12\left(1 - \nu_{xy}\nu_{yx}\right)}; \qquad D_y = \frac{E_y h^3}{12\left(1 - \nu_{xy}\nu_{yx}\right)}; \tag{3}$$

$$B = \frac{\nu_{xy} D_y}{2} + \frac{\nu_{yx} D_x}{2} + 2G_{xy} \frac{h^3}{12}. \tag{4}$$

The elastic constants ν_{xy} and ν_{yx} are related to the geometrical configuration of the orthotropic plate [31]. According to Betti's reciprocal theorem, the bending stiffness along the two principal directions satisfies the relationship [32]:

$$\nu_{yx} D_x = \nu_{xy} D_y. \tag{5}$$

A sound radiation model for an orthotropic thin plate has been developed using a general approach based on Hamilton's variational principle. The solution for the plate's transverse displacement w can be derived following the generalised approach proposed by Nelisse [6] to evaluate the sound power radiated by rectangular isotropic plates immersed in a fluid. The plate's transverse displacement $w(x, y, t)$ is approximated by a linear sum of admissible trial functions $\psi_{mn}(x, y)$:

$$w(x, y, t) = \sum_{m}^{M} \sum_{n}^{N} a_{mn} \psi_{mn}(x, y) \, \mathrm{e}^{\mathrm{i}\omega t}, \tag{6}$$

where a_{mn} represents the unknown amplitude of the transverse displacement associated with the mode (m, n). Assuming simply supported boundary conditions at all edges, sine functions can be used as trial functions $\psi_{mn}(x, y)$, providing numerical stability in the computation [33]:

$$\psi_{mn}(x, y) = \sin\left(\frac{m\pi x}{L_x}\right)\sin\left(\frac{n\pi y}{L_y}\right). \tag{7}$$

Assuming a harmonic time dependence of the kind $e^{\mathrm{i}\omega t}$, the plate steady state equation of motion for forced vibration can be expressed, for a given angular frequency ω, as a linear matrix system:

$$\left(-\omega^2 M_{mnpq} + K_{mnpq} + \mathrm{i}\omega Z_{mnpq}\right) a_{mn} = f_{mn}, \tag{8}$$

where M_{mnpq} are the mass matrix coefficients, K_{mnpq} the stiffness matrix coefficients, Z_{mnpq} are the coefficients of the impedance matrix, while f_{mn} are the coefficients of the external force vector. The amplitude coefficients a_{mn} of the transverse displacement vector $\mathbf{w}$ represents the only unknown of the system.

The stiffness matrix takes into account the orthotropic behaviour of the structure and its coefficients can generally be formulated as a double integral over the plate surface S:

$$\begin{aligned} K_{mnpq} = \int_0^{L_y}\int_0^{L_y} \Bigg[& D_x \frac{\partial^2}{\partial x^2}\psi_{mn}(x, y)\frac{\partial^2}{\partial x^2}\psi_{pq}(x, y) + D_y \frac{\partial^2}{\partial y^2}\psi_{mn}(x, y)\frac{\partial^2}{\partial y^2}\psi_{pq}(x, y) \\ & + \nu_{yx} D_x \frac{\partial^2}{\partial x^2}\psi_{mn}(x, y)\frac{\partial^2}{\partial y^2}\psi_{pq}(x, y) + \nu_{xy} D_y \frac{\partial^2}{\partial y^2}\psi_{mn}(x, y)\frac{\partial^2}{\partial x^2}\psi_{pq}(x, y) \\ & + 4G_{xy}\frac{h^3}{12}\frac{\partial^2}{\partial x \partial y}\psi_{mn}(x, y)\frac{\partial^2}{\partial x \partial y}\psi_{pq}(x, y)\Bigg] \mathrm{d}S. \end{aligned} \tag{9}$$

In Appendix A, the two-fold integral is reduced to a simpler and computationally faster formulation, under the assumption of simply-supported boundaries.

The mass matrix coefficients, as for an isotropic simply-supported plate, are given by:

$$M_{mnpq} = \rho h \int_0^{L_x}\int_0^{L_y} \sin\left(\frac{m\pi x}{L_x}\right)\sin\left(\frac{n\pi y}{L_y}\right)\sin\left(\frac{p\pi x}{L_x}\right)\sin\left(\frac{q\pi y}{L_y}\right) \mathrm{d}S. \tag{10}$$

However, due to the orthogonality property of the eigenfunctions, Eq. (10) reduces to:

$$M_{mnpq} = \begin{cases} M_{mn} = \dfrac{\rho h L_x L_y}{4}; & \text{if } m = p \text{ and } n = q, \\ 0; & \text{if } m \neq p \text{ or } n \neq q. \end{cases} \tag{11}$$

The radiation impedance $\mathbf{Z}$ is a sparse matrix of complex numbers. Its coefficients can be expressed in terms of its real and imaginary parts, the radiation resistance $\mathbf{R}$ and radiation reactance $\mathbf{X}$ respectively:

$$Z_{mnpq} = R_{mnpq} + \mathrm{i}X_{mnpq}. \tag{12}$$

The computation of the radiation impedance coefficients involves a four-fold integral to be solved:

$$Z_{mnpq} = \mathrm{i}\omega\rho_0 \int_S \int_S \psi_{mn}(x, y)\, G(x, y, 0, \overline{x}, \overline{y}, 0)\, \psi_{pq}(\overline{x}, \overline{y})\, \mathrm{d}S\, \mathrm{d}\overline{S}. \tag{13}$$

The Green's function $G(x, y, 0, \overline{x}, \overline{y}, 0)$ for the semi-infinite space is given by:

$$G(x, y, 0, \overline{x}, \overline{y}, 0) = \frac{\exp\left(-\mathrm{i}k_0 \sqrt{(x-\overline{x})^2 + (y-\overline{y})^2}\right)}{2\pi \sqrt{(x-\overline{x})^2 + (y-\overline{y})^2}}. \tag{14}$$

Eq. (13) has been reduced to a two-fold integral using the approach proposed by Sandman [4] and Nelisse [6], although by using different integration limits, as shown in Appendix B.

When the surrounding fluid has a low inertia compared to the radiating structure, the fluid loading and the modal cross-coupling are usually assumed to be negligible, as also shown in Appendix B. The coefficients of the radiation impedance matrix can thus be approximated by considering only the self-radiation resistance R_{mn}, i.e. the real part of the diagonal terms. The self-radiation resistance is proportional to the modal radiation efficiency σ_{mn} according to the relationship:

$$R_{mn} = n_{mn}\rho_0 c_0 S\, \sigma_{mn}, \tag{15}$$

where n_{mn} represents the norm of the mode, which in the case of simply-supported boundaries: $n_{mn} = 0.25$. The modal radiation efficiency σ_{mn} can be determined by using Wallace's formulation [34]:

$$\sigma_{mn} = \frac{64k_0^2 L_x L_y}{\pi^6 m^2 n^2} \int_0^{\pi/2} \int_0^{\pi/2} \left\{ \frac{\Gamma\left(\frac{\alpha}{2}\right) \Lambda\left(\frac{\beta}{2}\right)}{\left[\left(\frac{\alpha}{m\pi}\right)^2 - 1\right]\left[\left(\frac{\beta}{n\pi}\right)^2 - 1\right]} \right\}^2 \sin\theta\, \mathrm{d}\theta \mathrm{d}\phi, \tag{16}$$

in which $\alpha = k_0 L_x \sin\theta \cos\phi$ and $\beta = k_0 L_y \sin\theta \sin\phi$. The function Γ is cos if m is an odd integer, while it is sin if m is an even integer. The trigonometric functions for Λ are chosen analogously with respect to the integer n. The integration is performed over the propagation angle of the structural wave ϕ and over the angle of propagation θ of the acoustic wave in the fluid medium.

The coefficients associated with the external excitation are given, assuming a harmonic point-force, by:

$$f_{mn} = F_0 \psi_{mn}(x_S, y_S), \tag{17}$$

where F_0 represents an arbitrary amplitude of the point-force that drives the plate in the position (x_S, y_S).

Knowing the coefficients of the mass, stiffness, and radiation impedance matrix and of the external force vector, the amplitude of the plate's transverse displacement vector a_{mn} can be computed by solving a set of linear algebraic equations:

$$a_{mn} = A_{mnpq} f_{mn}, \tag{18}$$

where the admittance matrix $\mathbf{A}$ is obtained from the inversion of the matrices between parentheses on the left - hand side of equation (8) as:

$$A_{mnpq} = \left(-\omega^2 M_{mnpq} + K_{mnpq} + \mathrm{i}\omega Z_{mnpq}\right)^{-1}. \tag{19}$$

In order to numerically perform the matrix inversion, for each investigated frequency ω, it is necessary to re-arrange the multi-dimensional matrices $\mathbf{M}$, $\mathbf{K}$ and $\mathbf{Z}$, in two dimensions.

By solving Eq. (18) it is possible to compute the vibro-acoustic indicators as a function of the plate's transverse displacement w. The mean square vibration velocity of the plate is given by:

$$\left\langle v^2 \right\rangle = \frac{\omega^2}{8} \sum_m \sum_n |a_{mn}|^2 . \tag{20}$$

The radiated sound power is computed by integrating the active sound intensity over the plate surface:

$$W_{\mathrm{rad}} = \frac{\omega^2}{2} \sum_m \sum_n \sum_p \sum_q a_{mn} \mathrm{Re} \left[Z_{mnpq} \right] a^*_{pq}, \tag{21}$$

where the superscript * denotes the complex conjugate value. The orthotropic plate radiation efficiency can be determined according to Eq. (1).

2.2. Modal-average radiation efficiency

As the number of modes within the frequency band increases, it might be more convenient to derive an average radiation efficiency, rather than consider the radiation of each single mode. The modal-average radiation efficiency is an acoustic descriptor, usually expressed in one-third octave bands, often required in building acoustics, either in SEA-based prediction models and when a broad band excitation is involved. A statistical radiation efficiency model was implemented, based on the modal-average formulations proposed by Ghinet and Atalla [35] and by Anderson and Bratos-Anderson [36], using as input data frequency-dependent stiffness properties. Such a statistical approach requires some additional assumptions: (i) high modal density and modal overlap over the entire frequency range in order to treat the discrete distribution of modes as a continuous function; (ii) the sound power is only radiated by resonant modes; (iii) the resonant modes are uncorrelated; (iv) equipartition of modal energy can be applied: all the modes within the frequency band have the same vibrational energy. The average radiation efficiency of a thin orthotropic baffled panel can be computed by weighting the direction dependent radiation efficiency $\sigma(\omega, \phi)$ by the plate modal density n_d:

$$\sigma_{\mathrm{ortho}}(\omega) = \frac{L_x L_y}{\pi^2 n_d} \int_0^{\pi/2} \sigma(\omega, \phi)\, k_B \frac{\partial k_B}{\partial \omega}\, d\phi. \tag{22}$$

The radiation efficiency $\sigma(\omega, \phi)$ is computed, at a given angular frequency ω and propagation angle ϕ, using Leppington's asymptotic formulations [37, 38], developed for three different frequency ranges, with respect to the coincidence condition, which occurs when the acoustic wavenumber k_0 matches the wavenumber of the structural bending wave propagating in the plate k_B:

$$\begin{aligned} &\mu < 1 - \delta && \text{: above the critical condition;} \\ &\mu = 1 \pm \delta && \text{: near the critical condition;} \\ &\mu > 1 + \delta && \text{: below the critical condition;} \end{aligned}$$

where μ is the dimensionless bending wavenumber defined as the ratio: $\mu = \frac{k_B}{k_0}$. Below the critical condition the acoustic wavelength λ_0 is much bigger than the bending wavelength λ_B, vice-versa the acoustic wavenumber is smaller than the bending wavenumber. Air particles move parallel to the plate surface and compensate the oscillating areas associated with high and low pressure. Sound is only radiated at the edges, and at other discontinuities, where the pressure change cannot be fully compensated by the moving air. The radiation efficiency is much smaller than unity in this frequency range. Above the critical condition sound is radiated uniformly from the plate surface, like in the case of a piston source; therefore, the radiation efficiency approaches unity. The bending wavenumber k_B always fits the trace wavenumber of an acoustic wave propagating away from the surface at a certain angle: $k_B = k_0 \sin\theta$. At coincidence, $\mu = 1$, the plate radiates sound more efficiently than a piston source and σ exceeds unity. The complete set of equations to compute the asymptotic radiation efficiency is given in Leppington's papers [37, 38] where it was developed for an isotropic homogeneous plate. However, those papers do not provide information on how factor δ, which defines the frequency limits of the near-coincidence region, should be determined. The procedure we developed in order to determine the three frequency ranges for which Leppington's equations are defined was implemented for a discrete number of angles within the interval $0 \leq \phi \leq \pi/2$ and is described in Appendix C. Due to the orthotropic nature of the CLT plate, the bending wave velocity depends upon the propagation direction of the structural wave. Therefore, a direction-dependent bending wavenumber has to be considered. At any propagation angle ϕ, the direction-dependent bending wavenumber $k_B(\phi)$ can be estimated from the wavenumber components along the principal directions $k_{B,x}$ and $k_{B,y}$, by applying a well-established orthotropic elliptic model [39]:

$$k_B(\phi) = \sqrt{\left(k_{B,x}\cos\phi\right)^2 + \left(k_{B,y}\sin\phi\right)^2}. \tag{23}$$

For a thin orthotropic rectangular plate the modal density n_d, which describes the number of modes per Hertz, is given by:

$$n_d = \frac{L_x L_y \sqrt{\rho h}}{2\pi^2} \int_0^{\pi/2} \sqrt{\frac{1}{D(\phi)}}\, d\phi. \tag{24}$$

The direction-dependent bending stiffness $D(\phi)$ can be approximated for each propagation angle ϕ at a given angular frequency ω as:

$$D(\phi) = \frac{\omega^2 \rho h}{k_B^4(\phi)}. \tag{25}$$

This approximation might be helpful when information about the in-plane shear modulus G_{xy} is not available. Moreover, it is straightforward from Eq. (23) and Eq. (25) to determine the rate of change of the plate wavenumber with the frequency as:

$$k_B(\phi)\frac{\partial k_B}{\partial\omega} = \frac{\left(k_{B,x}\cos\phi\right)^2 + \left(k_{B,y}\sin\phi\right)^2}{2\omega}. \tag{26}$$

The frequency dependent stiffness properties required as input data in both models here presented can be derived from the bending wavenumbers $k_{B,x}$ and $k_{B,y}$ associated with the principal directions of the orthotropic plate.

3. Experimental measurements

Three different three-ply CLT plates, 4.2 m wide and 2.9 m high, were tested in Empa's wall sound insulation test facility. Even though all three panels are constituted by three plies of

Published article available online: https://doi.org/10.1016/j.apacoust.2018.08.022

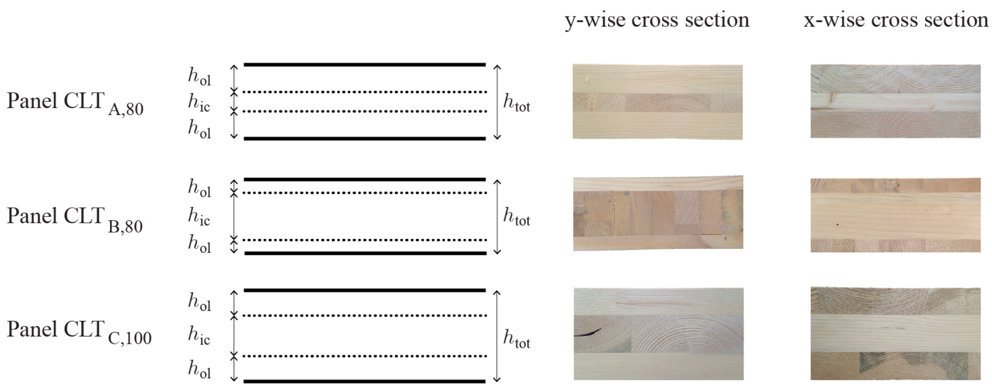

Figure 2: Investigated CLT panels: digram of the layers and cross-sections along the principal directions.

wooden beams, there are differences either in the ratio between the thickness of the inner core and the outer layers, or in the total thickness, as shown in Figure 2. The geometric characteristics of the tested panels are summarised in Table 1. Each plate was mounted in a rigid frame between the two testing rooms. It was fixed and sealed using elastic putty along all the edges on both sides, as shown in Figure 3. In order to experimentally evaluate the plate's radiation efficiency, one has to measure the mean square velocity of the plate surface and the total radiated sound power. A Polytec PSV-500 laser scanning vibrometer was used to measure the vibration velocity on a 513 points grid on the plate surface. The CLT wall was excited by a B&K 4809 vibration exciter driven with a white noise signal, to reproduce a structure-borne point source. In order to excite a sufficient number of modes two different source positions were used, one after the other, their coordinates p_{S_1} and p_{S_2} are given for each panel in Table 1. A PCB impedance-head was attached to the shaker stinger in order to determine the driving point mechanical impedance by measuring both the input force and the acceleration, from which the plate loss factor was evaluated. The diffuse field sound pressure in the receiving room was measured using a B&K rotating boom microphone. The radiated sound power cannot be directly measured, but needs to be determined from other quantities, such as sound pressure, sound intensity or vibration velocity. The sound power radiated from the tested CLT plates was experimentally determined by two different approaches.

Diffuse Field Approach (DFA) – Assuming a perfectly diffuse sound field, the radiated sound power is determined from the mean square sound pressure $\left\langle p^2 \right\rangle_{s,t}$, measured in the central area of the room. To account for the higher energy density near the room boundaries, which affects results at low frequencies, the Waterhouse correction [40] has been applied and the radiated

Table 1: Plate and test facility geometric characteristics

	$CLT_{A,80}$	$CLT_{B,80}$	$CLT_{C,100}$
L_x (m)	4.20	4.20	4.20
L_y (m)	2.90	2.90	2.90
S (m^2)	12.18	12.18	12.18
h_{tot} (m)	0.080	0.080	0.100
h_{ol} (m)	0.030	0.015	0.030
h_{ic} (m)	0.020	0.050	0.040
ρ (kg/m^3)	484.4	467.2	484.4
m' (kg/m^2)	38.75	37.38	48.44
$p_{S_1} = (x(\text{m}), y(\text{m}))$	$(0.5, 0.8)$	$(0.9, 1.2)$	$(0.5, 0.9)$
$p_{S_2} = (x(\text{m}), y(\text{m}))$	$(3.6, 0.9)$	$(3.2, 0.9)$	$(3.2, 1.2)$

power was calculated using the equation:

$$W_{\text{rad}} = \frac{\left\langle p^2 \right\rangle_{s,t}}{4\rho_0 c_0} A \left(1 + \frac{S_T \lambda_0}{8V}\right). \tag{27}$$

The absorption area A is calculated from the measured reverberation time and the room volume V using the well known Sabine's relation, λ_0 is the acoustic wavelength and S_T is the total surface area of the receiving room. The main limitation of this appraoch is the diffuse field assumption, which is hardly achieved below 100 Hz in wall sound insulation laboratories, designed according to the standard ISO 10140-5 [41].

Discrete Calculation Method (DCM) – The radiated sound power was also evaluated by using the DCM, as:

$$W_{\text{rad}} = \sum_i \left[\text{Re}\left(Z_{ii}\right) |v_i|^2 + \sum_j \text{Re}\left(Z_{ij} v_i v_j^*\right) \right]. \tag{28}$$

DCM is a hybrid method, proposed by Hashimoto [42], which requires both numerical calculations and the complex vibration velocity, measured over a grid of points on the plate surface. The plate surface has to be discretised in small piston-like source elements. The radiated sound power is determined from the calculated self- and cross-radiation impedances Z_{ii}, Z_{ij} and from the measured complex vibration velocity v_i of each sub-element. A complete and detailed description of this method is given in the original paper by Hashimoto [42]. In this method, it is assumed that the panel is surrounded by an infinite rigid baffle and that sound is radiated into a semi-infinite half-space. Effects due to the room's geometry are neglected.

The experimental radiation efficiency of the orthotropic CLT plate was used to validate the prediction models described in the previous section. The structural wavenumbers associated with the plate's principal directions $k_{B,x}$ and $k_{B,y}$, given in one-third octave band values in Table 2 and shown in narrowband in Figure 4, were experimentally determined from a non-destructive measurement procedure based on wave propagation analysis, described in detail in [43]. They were used to determine the stiffness properties required as model input data. Moreover, the plate

Published article available online: https://doi.org/10.1016/j.apacoust.2018.08.022

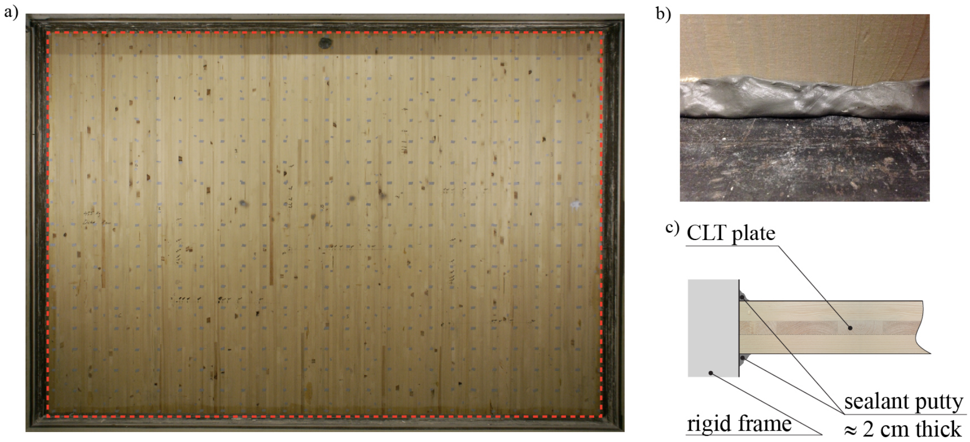

Figure 3: Experimental set-up: CLT plate mounted into a steel-concrete composite frame between the testing rooms of the sound transmission test facility.

damping can be taken into account, in both models, by means of complex input data [44]:

$$\overline{D} = D\,(1 + \mathrm{i}\eta)\,, \tag{29}$$

where $\overline{D}$ is the complex bending stiffness and η is the plate loss factor. The loss factor of the CLT plate was determined using the power injection method, as described in [45–47] from point input force and acceleration, measured with an impedance head attached to the shaker stinger. The accuracy of this approach has been proven in several papers [48–50], in which it was compared with other methods that can be used to determine the structural damping, such as the decay response method, or the half-power bandwidth method.

4. Results

The two prediction models are validated in this section by comparing the numerical results with the radiation efficiency experimentally measured for the three CLT plates. It is easier to understand the theoretical background underlying these models by deriving first the more general formulations and then simplifying the problem with more restrictive assumption. However, it is more convenient to present the results the other way around. At first the modal-average approach is considered, being the simplest and less computationally expensive; then the more accurate analytical/modal approach is validated. In both cases the experimental radiation efficiency is computed as the average of the results obtained from the DCM and the DFA approaches, which provide in general consistent results. A thorough investigation of their reliability can be found in [51], however, for sake of completeness, the panels' experimental radiation efficiency is plotted together with the standard deviation between the two methods. It should be mentioned that the DFA has not been applied below 100 Hz. It is shown that the experimental deviation between different approaches, or different source positions, can be up to 2-3 dB.

Table 2: One-third octave bands values of the structural wavenumbers and loss factor used as input data to model the cross-laminated timber plates

f (Hz)	$k_{B,x,\mathrm{CLT_{A80}}}$ (rad/m)	$k_{B,y,\mathrm{CLT_{A80}}}$ (rad/m)	$k_{B,x,\mathrm{CLT_{B80}}}$ (rad/m)	$k_{B,y,\mathrm{CLT_{B80}}}$ (rad/m)	$k_{B,x,\mathrm{CLT_{C100}}}$ (rad/m)	$k_{B,y,\mathrm{CLT_{C100}}}$ (rad/m)	η (-)
100	4.6	2.4	3.5	3.0	3.4	2.1	0.08
125	5.2	2.7	4.0	3.4	3.8	2.4	0.08
160	6.0	3.1	4.6	3.9	4.3	2.8	0.07
200	6.6	3.4	5.1	4.3	4.8	3.1	0.07
250	7.5	3.9	5.9	4.9	5.5	3.6	0.07
315	8.5	4.4	6.7	5.5	6.2	4.1	0.06
400	9.7	5.1	7.7	6.3	7.0	4.8	0.05
500	11.0	5.8	8.8	7.1	8.0	5.6	0.04
630	12.6	6.7	10.3	8.1	9.2	6.6	0.03
800	14.4	7.7	12.0	9.3	10.6	7.9	0.03
1000	16.7	9.0	14.1	10.7	12.2	9.4	0.03
1250	19.3	10.6	16.8	12.5	14.2	11.5	0.03
1600	22.5	12.5	20.2	14.5	16.6	14.0	0.03
2000	26.5	15.0	24.6	17.1	19.6	17.3	0.03
2500	31.4	18.2	30.1	20.3	23.4	21.6	0.03

4.1. Modal-average approach

The modal-average radiation efficiency computed for the three CLT plates is presented in Figures 5,6 and 7, in terms of radiation index $L_\sigma = 10\log\sigma$, in one-third octave bands. This statistical approach is validated by comparing the computed data with the radiation efficiency experimentally evaluated for each CLT panel by averaging the results obtained for the two shaker positions, thus no standard deviation is shown.

Orthotropic plates are characterised by a coincidence region limited by two coincidence frequencies, since the structural wave velocity depends on the propagation direction. The lowest coincidence frequency corresponds to the stiffest principal orthotropic direction and for CLT walls it is usually the vertical one, along which the outer layers' grains are oriented. As shown in the comparison in Figure 5, the predicted results well approximate the experimental radiation index measured for the plate $\mathrm{CLT_{A,80}}$. The first coincidence, indicated by a peak where the curve gradient changes, is found within the 250 Hz band, even though in the simulated data this is not as pronounced as in the experimental results. The upper coincidence frequency, which also represents the critical condition, is generally related to the horizontal principal direction of a CLT wall, perpendicular to the grain of the outer layers and parallel to the orientation of the core fibres. The critical condition of the plate $\mathrm{CLT_{A,80}}$ falls between the 800 Hz and 1000 Hz frequency bands. It is clearly identifiable by the curve maximum, which is more emphasised in the predicted radiation index than in the experimental results. Above the critical frequency the whole plate radiates sound like an ideal piston source and the radiation efficiency tends to unity. Similar findings have been obtained comparing calculated and measured results for the other two plates. The modal-average radiation efficiency computed for the plate $\mathrm{CLT_{B,80}}$ provides a good approximation of the experimental trend, as shown in Figure 6. This panel exhibits a weaker orthotropy, with its first coincidence between the 250 Hz and 315 Hz frequency bands and the critical condition in the band centred around 500 Hz. A similar agreement is also found between the simulated and experimental average-radiation efficiency of the plate $\mathrm{CLT_{C,100}}$, shown in Figure 7. The first coincidence falls in the 200 Hz frequency band, and the critical condition

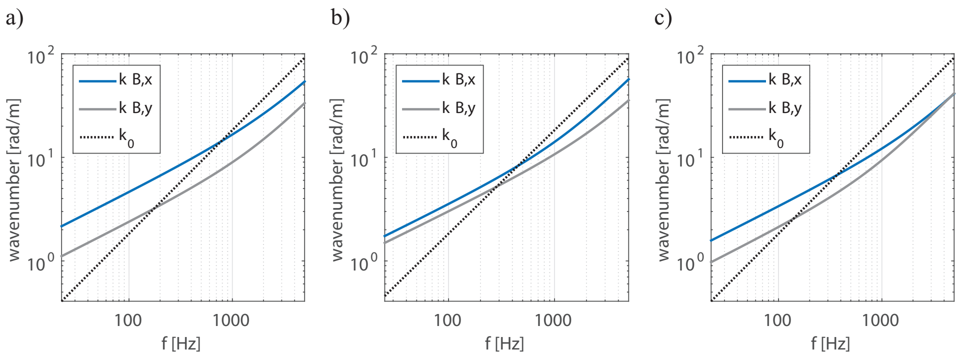

Figure 4: Structural wavenumbers along the principal directions used as input data to model the three CLT panels: (a) panel $CLT_{A,80}$; (b) panel $CLT_{B,80}$, (c) panel $CLT_{C,100}$

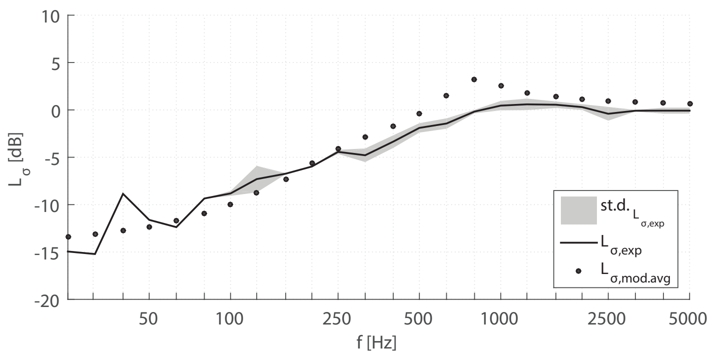

Figure 5: Panel $CLT_{A,80}$: the modal-average radiation index $L_{\sigma,\mathrm{mod-avg}}$ is compared with the experimental results averaged over all the source positions $L_{\sigma,\mathrm{exp}}$ in one-third octave bands.

is between the bands centred around 400 Hz and 500 Hz. Once again the numerical radiation efficiency well approximates the trend of the experimental data providing a smooth curve with the peak associated with the critical condition spread over different frequency bands and the first coincidence pinpointed by a change in the curve slope.

In general, such a statistical model allows to obtain a good approximation of the radiation efficiency trend in the considered frequency range, identifying with good accuracy the first coincidence and the critical condition; although it cannot provide a very accurate and detailed prediction below the critical condition. The high modal density assumption, necessary to consider a continuous distribution of modes, is not sufficiently fulfilled within the entire frequency range, since below the critical condition the vibrational field of the CLT plate surface is not perfectly diffuse and only a few modes lay within the frequency bands. Moreover, the near-field generated around the excitation point represents a discontinuity, not considered by the model, which usually enhance radiation. Nevertheless, the modal-average approach provides helpful insights on the radiation of the orthotropic CLT plate, even if it is not able to capture the modal behaviour

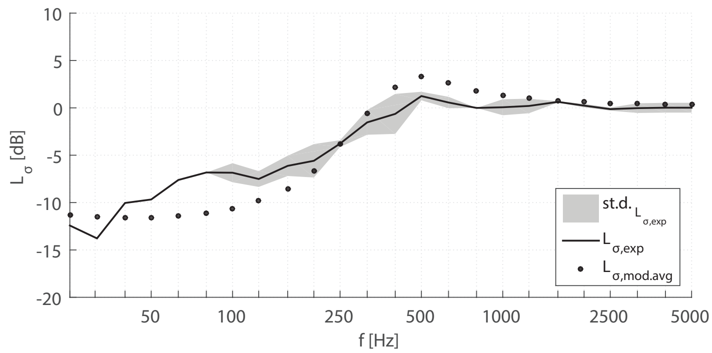

Figure 6: Panel $\mathrm{CLT}_{\mathrm{B},80}$: the modal-average radiation index $L_{\sigma,\mathrm{mod-avg}}$ is compared with the experimental results averaged over all the source positions $L_{\sigma,\mathrm{exp}}$ in one-third octave bands.

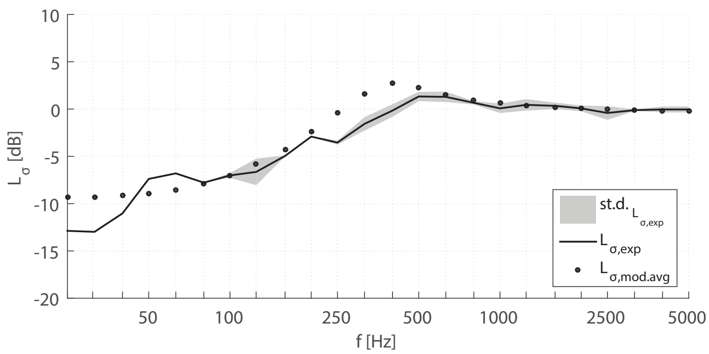

Figure 7: Panel $\mathrm{CLT}_{\mathrm{C},100}$: the modal-average radiation index $L_{\sigma,\mathrm{mod-avg}}$ is compared with the experimental results averaged over all the source positions $L_{\sigma,\mathrm{exp}}$ in one-third octave bands.

below the critical frequency.

4.2. Modal / analytical approach

A vibro-acoustic model based on an modal/analytical approach has been implemented with the aim to obtain a more detailed prediction also in the frequency region characterised by a low mode count. Moreover, this approach also allows to take into account the influence of the fluid loading, even though the computation of the radiation impedance matrix requires a huge effort. However, the influence of fluid loading on the sound radiated by a CLT building panel is very small, as proven in Appendix B, since air has a much lower inertia compared to the investigated structures. Therefore, the radiation impedance can be approximated by the real part of the self-radiation resistance, neglecting fluid loading and reducing significantly the computational cost of the algorithm. The model is validated by comparing the numerical results with the experimental CLT plates' radiation efficiency for each single shaker position. In Figure 8 the numerical and experimental results for the panel $\mathrm{CLT}_{\mathrm{A},80}$ are compared. The graph *(a)*, on the

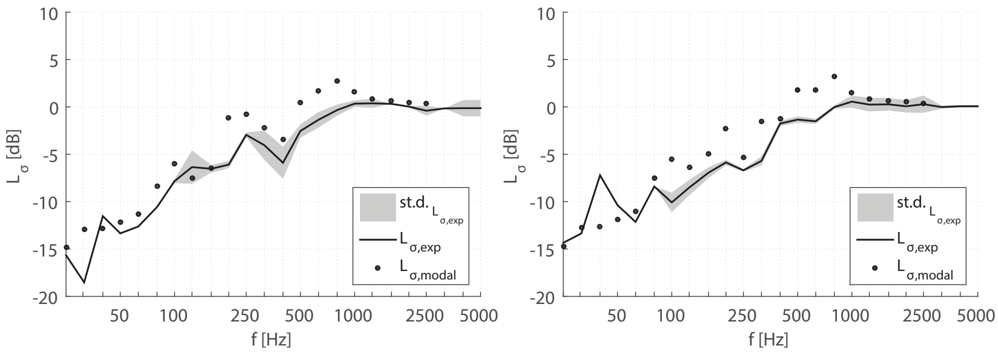

Figure 8: Panel $\mathrm{CLT}_{A,80}$: modal based radiation index in one-third octave bands. Comparison between numerical results and experimental data: (a) plate mechanically excited at position p_{S_1}; (b) plate mechanically excited at position p_{S_2}.

left-hand side, refers to source position p_{S_1}, while the graph *(b)* on the right-hand side is related to source position p_{s_2}. Given that experimental deviations can be up to 2-3 dB, the comparisons show good agreement between numerical and experimental results, despite the fact that the predicted radiation efficiency is overestimated in certain frequency bands with discrepancies up to 5 dB. Below the critical condition the dips and peaks of experimental radiation efficiency are approximated with good accuracy by the predicted results. The comparison between the predicted and experimental radiation efficiency of the panel $\mathrm{CLT}_{B,80}$, shown in Figure 9 highlights a good agreement. However, as for the previous panel, the simulated radiation efficiency is, in certain bands, slightly overestimated or some peaks associated with the structural resonant modes can be shifted towards neighbouring frequency bands. The same conclusions can be drawn from the comparison between numerical and experimental radiation efficiency of the panel $\mathrm{CLT}_{C,100}$, given in Figure 10. In this case slightly larger discrepancies are found, especially in the very low frequencies, but still the numerical radiation efficiency well approximates the measured data.

It should be noted that the spread in the experimental radiation efficiency, expressed as standard deviation, is for some frequency band significant and comparable to the difference between measured and predicted results. Moreover, below the upper coincidence frequency, i.e. the critical condition, the sound is mainly radiated from the plate discontinuities, such as the boundaries. The real mounting conditions, described in section 3, are much more complex than the simply-supported boundaries assumed in the model: at the bottom edge the plate is supported by a rigid frame whereas at all the other edges there is a small gap, sealed with elastic putty. These edge mountings cannot completely prevent the out-of-plane translational motion of the plate, as required by the assumption of simply-supported boundaries, resulting as a lower degree of restraint. The difference between theoretical and real boundary conditions is the main cause of the discrepancies between predicted and experimental radiation efficiency. In fact, according to a recent study presented by Squicciarini et al. [52], in which the radiation efficiency of a plate with different combinations of boundary condition was investigated, differences up to 25 dB can be found between totally free and simply-supported boundaries. The study highlights the general trend of a diminishing radiation efficiency as the degree of restraint at the edges decreases. A more rigorous model, considering mixed boundary conditions with translational and rotational

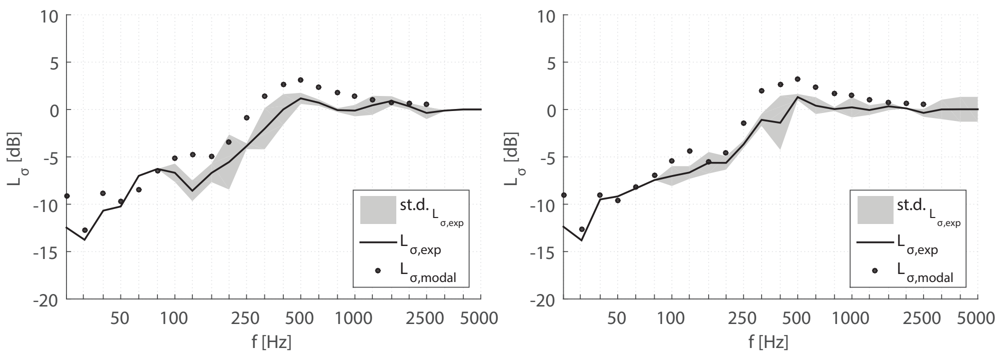

Figure 9: Panel $\mathrm{CLT}_{\mathrm{B},80}$: modal based radiation index in one-third octave bands. Comparison between numerical results and experimental data: (a) plate mechanically excited at position p_{S_1}; (b) plate mechanically excited at position p_{S_2}.

springs with very uncertain and locally varying stiffness, would require a tremendous effort that would not have practical applicability. Therefore, in order to develop a usable tool for building acoustics design, simply-supported boundaries have been considered, since they allow for an analytical closed solution reducing the algorithm's computational cost.

4.3. Comparison between the two models

The results obtained from the two models presented provide constent results in reasonably good agreement with the experimental data. However, in both cases some discrepancies were found, either in the low frequency range, or at higher freqeuncies where the models seems to slightly overestimate the radiation index around the critical condition. This effect, which was also observed in an analogous investigation of sound transmission loss of CLT panels [53], is probably related to the damping of the system, even though it was taken into consideration in the models by means of a complex stiffness, as given in Eq. (29). However, for a complete understanding of the problem a further investigation is required in future works. A last comparison is made between the results obtained from the two different prediction approaches. In Figure 11 a), the modal-average radiation index $L_{\sigma,mod.avg}$ of the plate $\mathrm{CLT}_{\mathrm{A},80}$ is compared, in one-third octave bands, to the two radiation indexes, computed by using a modal/analytical approach for each source position used in the experiments: $L_{\sigma,modal,S_1}$ and $L_{\sigma,modal,S_2}$. While the two models provide a consistent trend, the modal-based radiation indexes associated with the two excitation sources highlight peaks and dips associated with the structural modes up to approximately 500 Hz. In order to consider a higher number of modes excited in the plate, the modal radiation index of the panel $\mathrm{CLT}_{\mathrm{A},80}$, was averaged over 100 non-simultaneous source positions, randomly chosen over the plate surface. In Figure 11 b), the modal radiation index averaged over 100 source positions $L_{\sigma,mod,100}$ is compared to the statistical results $L_{\sigma,mod.avg}$. By increasing the number of excited modes the structural modal behaviour is noticeable only up to the 250 Hz band, while at higher frequencies the radiation curve smooths out. Moreover, the statistical radiation index seems to underestimate the results obtained from the modal approach within all the frequency bands below the critical condition, in all probability due to the low mode count in this frequency range.

Published article available online: https://doi.org/10.1016/j.apacoust.2018.08.022

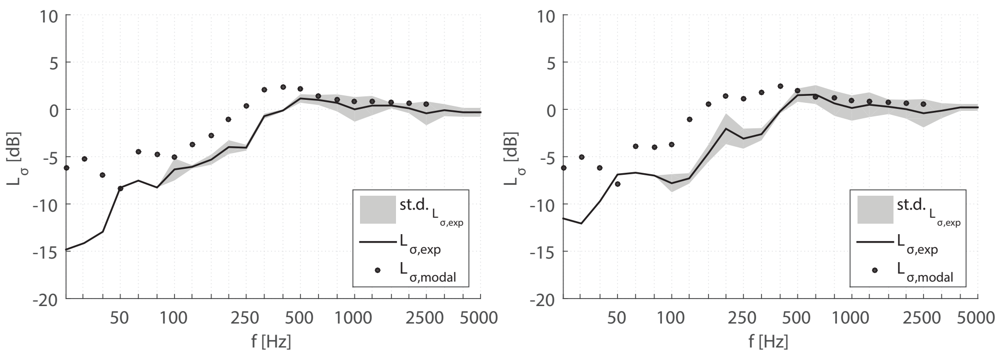

Figure 10: Panel $\mathrm{CLT}_{\mathrm{C},100}$: modal based radiation index in one-third octave bands. Comparison between numerical results and experimental data: (a) plate mechanically excited at position ps_1; (b) plate mechanically excited at position ps_2.

The modal-average approach is a handy computationally efficient tool, for preliminary investigations, in order to obtain information on the radiation trend, or on the coincidence frequencies of an orthotropic panel. However, it may lead to underestimated results if the mode count within a certain frequency band is low, since the basic assumption of high modal density is not fulfilled. In this case, a more accurate approximation of the radiation efficiency can be obtained by means of a modal approach which considers all the modes actually excited by the source, even though it requires a greater computational effort.

5. Conclusion

Two models to evaluate the radiation efficiency of a CLT panel, developed with different approaches, have been presented. In both models the panel is assumed to be a baffled thin orthotropic plate with simply supported boundary conditions, excited by a broad band, mechanical force. These models have been validated with the experimental radiation efficiency of three mechanically-excited three-ply cross-laminated timber plates, which was determined by using two different methods to evaluate the total radiated sound power: the diffuse field approach (DFA) and the discrete calculation method (DCM), which provided consistent results.

A modal-average approach provides a good approximation of the radiation efficiency trend. However, if the vibrational field is not diffuse, but only few modes exist within a frequency band, it is not suitable for an accurate prediction below the critical condition, since some of the basic assumptions the model is based on, such as high modal density and continuous distribution of modes, are not fulfilled within this frequency range. Nevertheless, it still represents a simple and useful tool to perform preliminary analysis on orthotropic plates during the design process. The two shaker positions used to experimentally evaluate the CLT panel's radiation efficiency provided results significantly different in the low frequency range. It should be noted that in-situ building walls can be excited by multiple and rather complex sources simultaneously; this condition would thus extend towards lower frequencies the range in which the assumption of diffuse vibrational field is fulfilled.

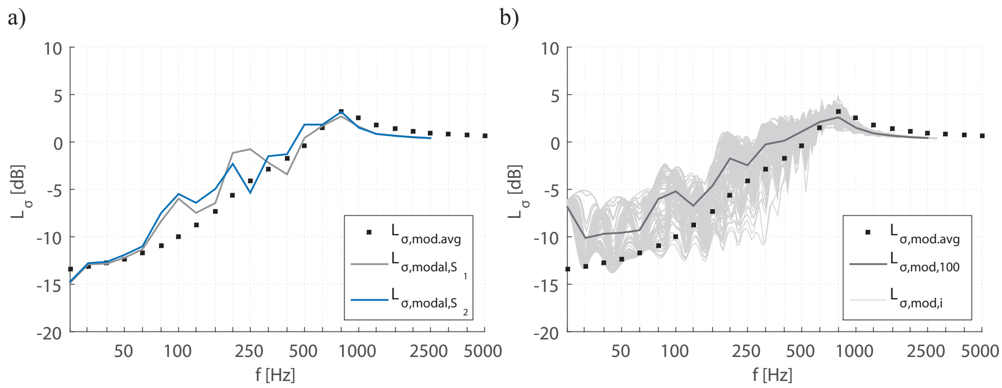

Figure 11: Comparison between the two different approaches: a) the radiation index obtained from modal average approach is compared with the radiation indexes computed with the modal/analytical approach for the two source positions; b) the radiation index obtained from modal average approach is compared with the radiation index, obtained using the modal approach and averaged over 100 source positions.

For a more accurate and detailed prediction of the radiation efficiency of orthotropic plates, even below the critical condition, a modal/analytical approach has been presented. The assumption of simply-supported boundaries allows for an analytical or approximated closed solution of most of the integral equations involved in the model, providing a fast algorithm. Moreover, the influence of the fluid loading on the sound radiated in the surrounding air by a CLT panel has been proven to be very small. It can thus be neglected by approximating the radiation impedance with the real part of the self radiation resistance, reducing significantly the computational cost of the algorithm. A good agreement between predicted and experimental results was found, although the model slightly overestimates the radiation efficiency experimentally evaluated for the tested CLT plate, particularly below the critical condition. Boundary conditions have a significant influence on sound radiation in this frequency range. In fact, these discrepancies are mostly due to the difference between the constraint provided by the real mounting conditions and the idealised simply supported boundaries. However, the simply-supported boundaries assumption allows one to obtain a sufficiently good approximation of the radiation efficiency in a reasonable time. The modal / analytical approach requires a greater computational effort compared to the statistical model, but it provides an accurate approximation of the radiation efficiency of a CLT panel even below the critical condition, where such a structure is characterised by a rather low modal density. Further uncertainty can possibly be due to the experimental wavenumbers used as input data for the material's elastic properties. However, the agreement highlighted by the presented results proved that by means of frequency dependent properties it is possible to treat complex structures, such as CLT panels, as homogeneous elements. The structural wavenumbers can be experimentally determined in a number of ways. The determination of the structural wavenumber, or at least of its real part, seems straightforward if compared to the effort required in order to determine all the characteristics that would be necessary to consider otherwise, such as the properties of wooden beams and their connection within each ply as well as the coupling between the different plies that constitute the CLT panel.

Published article available online: https://doi.org/10.1016/j.apacoust.2018.08.022

Acknowledgement

All the experimental measurements and most of the data analysis have been performed at *Empa - Swiss Federal Laboratories for Material Science and Technology - Laboratory for Acoustics/Noise Control*.

Appendix A. Stiffness matrix

In this paragraph the equation to compute the stiffness matrix coefficients is derived for the case of simply-supported boundary conditions. Using the dimensionless coordinates:

$$\begin{cases} u = \dfrac{x}{L_x}; \\ v = \dfrac{y}{L_y}. \end{cases}$$

Eq. (9) is rewritten in terms of the new spatial coordinates u and v:

$$\begin{aligned} K_{mnpq} =& L_x L_y \int_0^1 \int_0^1 \left[D_x \left(\frac{1}{L_x^2} \right)^2 \frac{\partial^2}{\partial u^2} \psi_{mn}(u,v) \frac{\partial^2}{\partial u^2} \psi_{pq}(u,v) \right. \\ & + D_y \left(\frac{1}{L_y^2} \right)^2 \frac{\partial^2}{\partial v^2} \psi_{mn}(u,v) \frac{\partial^2}{\partial v^2} \psi_{pq}(u,v) \\ & + \nu_{yx} D_x \left(\frac{1}{L_y L_x} \right)^2 \frac{\partial^2}{\partial u^2} \psi_{mn}(u,v) \frac{\partial^2}{\partial v^2} \psi_{pq}(u,v) \\ & + \nu_{xy} D_y \left(\frac{1}{L_y L_x} \right)^2 \frac{\partial^2}{\partial v^2} \psi_{mn}(u,v) \frac{\partial^2}{\partial u^2} \psi_{pq}(u,v) \\ & \left. + 4 G_{xy} \frac{h^3}{12} \left(\frac{1}{L_y L_x} \right)^2 \frac{\partial^2}{\partial u \partial v} \psi_{mn}(u,v) \frac{\partial^2}{\partial u \partial v} \psi_{pq}(u,v) \right] \mathrm{d}v \mathrm{d}u, \end{aligned} \tag{A.1}$$

the mode shape functions for simply-supported boundaries are given in the new coordinate system as:

$$\begin{cases} \psi_{mn}(u,v) = \sin(m\pi u) \sin(n\pi v); \\ \\ \psi_{pq}(u,v) = \sin(p\pi u) \sin(q\pi v). \end{cases}$$

Due to the orthogonal property of the basis functions Eq. (A.1) can be reduced to:

- if $m = p$ and $n = q$

$$K_{mnpq} = K_{mn} = \frac{L_x L_y}{4} \left[D_x \frac{m^4 \pi^4}{L_x^4} + D_y \frac{n^4 \pi^4}{L_y^4} + 2B \frac{m^2 n^2 \pi^4}{L_x^2 L_y^2} \right]; \tag{A.2}$$

- if $m \neq p$ and $n \neq q$

$$K_{mnpq} = 0. \tag{A.3}$$

The stiffness matrix is hence diagonal and can be computed as an algebraic equation, significantly reducing the computational time.

The apparent bending stiffness along each principal i-direction D_i is obtained according to Eq. (3) from the experimental wavenumbers $k_{B,x}$ and $k_{B,y}$ given in Table 2. The in-plane shear modulus G_{xy} of the orthotropic plate, necessary to compute the effective torsional stiffness B given in equation (4), has been approximated as a function of the elastic moduli associated with the principal directions [32] as:

$$G_{xy} = \frac{\sqrt{E_x E_y}}{2\left(1 + \sqrt{\nu_{xy}\nu_{yx}}\right)}. \tag{A.4}$$

The value of the elastic properties ν_{xy} and ν_{xy}, has been determined by considering Eq. (5) and assuming the Poisson's ratio $\nu = \sqrt{\nu_{xy}\nu_{yx}} = 0.3$ as typical for wood materials. The apparent frequency dependent elastic properties E_x and E_y have been derived from the bending stiffness along the principal directions D_x and D_y according to Eq. (3).

Appendix B. Radiation impedance matrix

For a simply-supported baffled plate, the four-fold integral equation to compute the radiation impedance given in Eq. (13) is reduced to a double integral by using the approximation proposed by Sandman [4] and Nellisse [6]. A first coordinate transform is applied:

$$\begin{cases} \alpha = \dfrac{x}{L_x}; \\ \\ \beta = \dfrac{y}{L_y}; \end{cases} \qquad \begin{cases} \overline{\alpha} = \dfrac{\overline{x}}{L_x}; \\ \\ \overline{\beta} = \dfrac{\overline{y}}{L_y}; \end{cases} \qquad r = \frac{L_x}{L_y}.$$

After the mode mixing the radiation impedance results:

$$Z_{mnpq} = i\omega\rho_0 S^2 \int_0^1 \int_0^1 \int_0^1 \int_0^1 \psi_{mp}\left(\alpha, \overline{\alpha}\right) G\left(\alpha, \beta, 0, \overline{\alpha}, \overline{\beta}, 0\right) \psi_{nq}\left(\beta, \overline{\beta}\right) \, \mathrm{d}\overline{\alpha} \, \mathrm{d}\overline{\beta} \, \mathrm{d}\alpha \, \mathrm{d}\beta. \tag{B.1}$$

To reduce the four-fold integral another change of variable is needed:

$$\begin{cases} u = \alpha - \overline{\alpha}; \\ \\ v = \overline{\alpha}; \end{cases} \qquad \begin{cases} \overline{u} = \beta - \overline{\beta}; \\ \\ \overline{v} = \overline{\beta}. \end{cases}$$

Considering the symmetry of the mode shape functions, the radiation impedance can be expressed as:

$$Z_{mnpq} = i\omega\rho_0 4S^2 \int_0^1 \int_0^1 \Phi_{mp}\left(u\right) G\left(u, 0, \overline{u}, 0\right) \Phi_{nq}\left(\overline{u}\right) \, \mathrm{d}\overline{u} \, \mathrm{d}u, \tag{B.2}$$

where:

$$\Phi_{mp}(u) = \int_0^{1-u} \sin(m\pi(u+v))\sin(p\pi v)\,\mathrm{d}v;$$

$$\Phi_{nq}(\overline{u}) = \int_0^{1-\overline{u}} \sin(n\pi(\overline{u}+\overline{v}))\sin(q\pi\overline{v})\,\mathrm{d}\overline{v}; \tag{B.3}$$

$$G(u,0,\overline{u},0) = \frac{\exp\left(-\mathrm{i}k_0 L_x \sqrt{u^2 - r^{-2}(\overline{u})^2}\right)}{2\pi L_x \sqrt{u^2 - r^{-2}(\overline{u})^2}}.$$

Seeking a solution for the integral functions $\Phi_{mp}(u)$ and $\Phi_{nq}(\overline{u})$ it is possible to write:

- if $m = p$ and $n = q$:

$$\begin{aligned} \Phi_{mp}(u) &= \frac{\sin(\pi m(u-2))}{4\pi m} + \frac{\sin(\pi m u)}{4\pi m} + \cos(\pi m u)\left(\frac{1-u}{2}\right); \\ \Phi_{nq}(\overline{u}) &= \frac{\sin(\pi n(\overline{u}-2))}{4\pi n} + \frac{\sin(\pi n\overline{u})}{4\pi n} + \cos(\pi n\overline{u})\left(\frac{1-\overline{u}}{2}\right). \end{aligned} \tag{B.4}$$

- if $m \neq p$ and $n \neq q$:

$$\begin{aligned} \Phi_{mp}(u) &= \frac{\sin(\pi(m-p+pu))}{2\pi(m-p)} - \frac{\sin(\pi m u)}{2\pi(m-p)} - \frac{\sin(\pi(m+p-pu))}{2\pi(m+p)} + \frac{\sin(\pi m u)}{2\pi(m+p)}; \\ \Phi_{nq}(\overline{u}) &= \frac{\sin(\pi(n-q+q\overline{u}))}{2\pi(n-q)} - \frac{\sin(\pi n\overline{u})}{2\pi(n-q)} - \frac{\sin(\pi(n+q-q\overline{u}))}{2\pi(n+q)} + \frac{\sin(\pi n\overline{u})}{2\pi(n+q)}; \end{aligned} \tag{B.5}$$

Applying Prosthaphaeresis' sum to product formulas, Eq. (B.5) and Eq. (B.4) can be reformulated as:

- if $m = p$ and $n = q$:

$$\begin{aligned} \Phi_{mp}(u) =& \frac{1}{\pi}\left\{\frac{\cos\left(\frac{\pi(m-p)}{2} + \frac{\pi(m+p)u}{2}\right)\sin\left(\frac{\pi(m-p)}{2} - \frac{\pi(m-p)u}{2}\right)}{m-p}\right. \\ & \left. - \frac{\cos\left(\frac{\pi(m+p)}{2} + \frac{\pi(m-p)u}{2}\right)\sin\left(\frac{\pi(m+p)}{2} - \frac{\pi(m+p)u}{2}\right)}{m+p}\right\}; \\ \Phi_{nq}(\overline{u}) =& \frac{1}{\pi}\left\{\frac{\cos\left(\frac{\pi(n-q)}{2} + \frac{\pi(n+q)\overline{u}}{2}\right)\sin\left(\frac{\pi(n-q)}{2} - \frac{\pi(n-q)\overline{u}}{2}\right)}{n-q}\right. \\ & \left. - \frac{\cos\left(\frac{\pi(n+q)}{2} + \frac{\pi(n-q)\overline{u}}{2}\right)\sin\left(\frac{\pi(n+q)}{2} - \frac{\pi(n+q)\overline{u}}{2}\right)}{n+q}\right\}; \end{aligned} \tag{B.6}$$

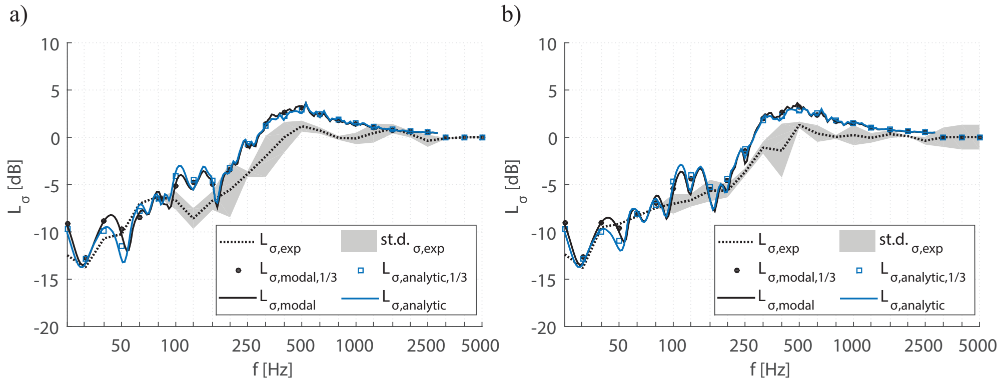

Figure B.12: Comparison between radiation efficiency of the panel $\mathrm{CLT}_{\mathrm{B},80}$ either computed considering the radiation impedance coefficients Z_{mnpq} and its approximation with the self radiation resistance coefficients R_{mn}: (a) plate mechanically-excited at position p_{S_1}; (b) plate mechanically-excited at position p_{S_2}.

- if $m = p$ and $n = q$:

$$\Phi_{mp}(u) = \frac{1}{2\pi m}\left[\sin(\pi m(u-1))\cos(-\pi m)\right] + \cos(\pi m u)\left(\frac{1-u}{2}\right);$$
$$\Phi_{nq}(\bar{u}) = \frac{1}{2\pi n}\left[\sin(\pi n(\bar{u}-1))\cos(-\pi n)\right] + \cos(\pi n\bar{u})\left(\frac{1-\bar{u}}{2}\right). \tag{B.7}$$

The radiation indices, computed considering both the full radiation impedance matrix Z_{mnpq}, indicated as $L_{\sigma,\mathrm{analytic}}$, and its approximation with the self-radiation resistance R_{mn}, $L_{\sigma,\mathrm{modal}}$, are compared in narrow band in Figure B.12 for two positions of the mechanical point excitation, only the panel $\mathrm{CLT}_{\mathrm{B},80}$, since it has the lowest surface mass. At low frequencies fluid loading has a small influence on sound radiated by a CLT plate and it is even smaller in the mid-high frequency range. We can conclude that although CLT panels are lightweight elements compared to the traditional building partitions, their inertia is still several orders of magnitude larger than the one provided by air, thus the load of the fluid does not affect significantly the plate dynamics.

Appendix C. Near-coincidence frequency range: $\mu \approx 1 \pm \delta$

In order to compute the modal-average radiation efficiency it is necessary to define three regions for which Leppington's equations are defined. In the implemented algorithm these intervals are not set a priori, instead all the three curves are computed for each investigated propagation direction ϕ. The function defined in the *above-coincidence (ac)* range assumes negative values below the critical condition while it is positive and tends asymptotically to unity above. The function defined in the *below-coincidence (bc)* region presents a discontinuity at the first coincidence where $\mu = 1$. The first formulation presented by Leppington could not solve this singularity for $\mu = 1$, but some years later he proposed an integral formulation for a positive and continuous function valid within a region around the coincidence frequency, the *near-coincidence (nc)* interval. The cut-off frequency between the *bc* and *nc* regions is identified by the intersection which

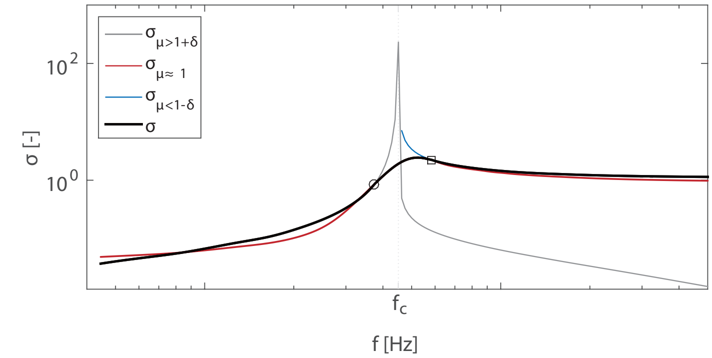

Figure C.13: Determination of the average radiation efficiency for a single propagation direction by combining the curves defined in each frequency region: below-coincidence, near-coincidence, above-coincidence;

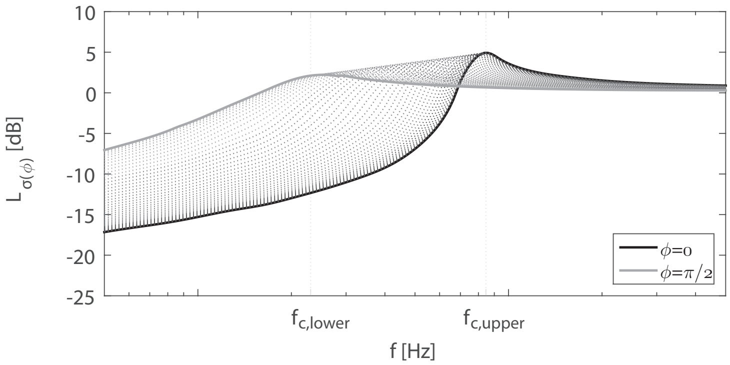

Figure C.14: Frequency dependent average radiation index for different propagation angles ϕ.

is the closest to the discontinuity of the *bc* function. The first intersection between the *nc* function and the *ac* positive curve represents the limit between these two regions. It might happen that, due to numerical reasons, two curves do not intersect each other, even though the transition between two regions occurred. In this case the implemented algorithm evaluates the frequency at which the two functions are closest to each other. Once those limits are defined the resulting radiation efficiency is determined, for each investigated angle, by combining the three curves within the frequency range in which they are respectively defined. In Figure C.14 the radiation index is plotted, from $\phi = 0$ to $\phi = \pi/2$ at steps of $\Delta\phi = \pi/90$. The radiation efficiency with the lowest coincidence frequency is determined for the bending wave propagating along the stiffest direction, while the curve with the highest critical frequency is associated with the orthogonal direction. In other words the critical condition is shifted towards lower frequencies as the plate stiffness increases.

References

[1] F. Fahy, P. Gardonio, Sound and Structural Vibration. Radiation, Transmission and Response, 2nd Edition, Academic Press in an imprinting of Elsevier, Oxford, UK, 2007.

[2] G. Maidanik, Response of ribbed panels to reverberant acoustic fields, The Journal of the Acoustical Society of America 34 (6) (1962) 809–826.

[3] A. Berry, J. L. Guyader, J. Nicolas, A general formulation for the sound radiation from rectangular, baffled plates with arbitrary boundary conditions, The Journal of the Acoustical Society of America 88 (6) (1990) 2792–2802.

[4] B. E. Sandman, Motion of a three-layered elastic–viscoelastic plate under fluid loading, The Journal of the Acoustical Society of America 57 (5) (1975) 1097–1107.

[5] N. Atalla, J. Nicolas, A new tool for predicting rapidly and rigorously the radiation efficiency of plate-like structures, The Journal of the Acoustical Society of America 95 (6) (1994) 3369–3378.

[6] H. Nelisse, O. Beslin, J. Nicolas, A generalized approach for the acoustic radiation from a baffled or unbaffled plate with arbitrary boundary conditions, immersed in a light or heavy fluid, Journal of Sound and Vibration 211 (2) (1998) 207–225.

[7] O. Foin, J. Nicolas, N. Atalla, An efficient tool for predicting the structural acoustic and vibration response of sandwich plates in light or heavy fluid, Applied Acoustics 57 (3) (1999) 213–242.

[8] A. Mejdi, N. Atalla, Dynamic and acoustic response of bidirectionally stiffened plates with eccentric stiffeners subject to airborne and structure-borne excitations, Journal of Sound and Vibration 329 (21) (2010) 4422–4439.

[9] J. Legault, A. Mejdi, N. Atalla, Vibro-acoustic response of orthogonally stiffened panels: The effects of finite dimensions, Journal of Sound and Vibration 330 (24) (2011) 5928–5948.

[10] D. Rhazi, N. Atalla, Transfer matrix modeling of the vibroacoustic response of multi-materials structures under mechanical excitation, Journal of Sound and Vibration 329 (13) (2010) 2532–2546.

[11] J. L. Davy, The forced radiation efficiency of finite size flat panels that are excited by incident sound, The Journal of the Acoustical Society of America 126 (2) (2009) 694–702.

[12] J. L. Davy, D. J. Larner, R. R. Wareing, J. R. Pearse, The average specific forced radiation wave impedance of a finite rectangular panel, The Journal of the Acoustical Society of America 136 (2) (2014) 525–536.

[13] J. L. Davy, D. J. Larner, R. R. Wareing, J. R. Pearse, The acoustic radiation impedance of a rectangular panel, Building and Environment 92 (2015) 743–755.

[14] B. Zeitler, S. Schoenwald, I. Sabourin, Direct impact sound insulation of cross laminate timber floors with and without toppings, in: Proceedings of the 43^{nd} International Congress and Exposition on Noise Control Engineering, Vol. 249, Institute of Noise Control Engineering, Melbourne, Australia, 2014, pp. 5742–5747.

[15] L. Barbaresi, F. Morandi, M. Garai, A. Speranza, Experimental measurements of flanking transmission in CLT structures, in: Proceedings of Meetings on Acoustics, 22^{nd} ICA, Vol. 28, ASA, 2016, p. 015015.

[16] A. Di Bella, N. Granzotto, L. Barbaresi, Analysis of acoustic behaviour of bare CLT floors for the evaluation of impact sound insulation improvement, in: Proceedings of Meetings on Acoustics, 22^{nd} ICA, Vol. 28, ASA, 2016, p. 015016.

[17] M. Caniato, F. Bettarello, P. Fausti, A. Ferluga, L. Marsich, C. Schmid, Impact sound of timber floors in sustainable buildings, Building and Environment 120 (2017) 110–122.

[18] M. Caniato, F. Bettarello, A. Ferluga, L. Marsich, C. Schmid, P. Fausti, Acoustic of lightweight timber buildings: A review, Renewable and Sustainable Energy Reviews 80 (2017) 585–596.

[19] S. Schoenwald, B. Zeitler, I. Sabourin, F. King, Sound insulation performance of cross laminated timber building systems, in: Proceedings of the 42^{nd} International Congress and Exposition on Noise Control Engineering, Institute of Noise Control Engineering, Innsbruck, Austria, September 2013.

[20] B. Van Damme, S. Schoenwald, M. Alvarez Blanco, A. Zemp, Limitation to the use of homogenized material parameters of cross laminated timber plates for vibration and sound transmission modelling, in: Proceedings of the 22^{nd} International Congress on Sound and Vibration, International Institute of Acoustics and Vibration, Florence, Italy, 2015.

[21] B. Van Damme, S. Schoenwald, A. Zemp, Modeling the bending vibration of cross-laminated timber beams, European Journal of Wood and Wood Products 75 (6) (2017) 985–994.

[22] ISO 12354-1 – Building acoustics: Estimation of acoustic performance of buildings from the performance of elements – Part 1: Airborne sound insulation between rooms, Standard, International Organization for Standardization, Geneva, CH (2017).

[23] A. Santoni, P. Bonfiglio, J. L. Davy, P. Fausti, F. Pompoli, L. Pagnoncelli, Sound transmission loss of *ETICS* cladding systems considering the structure-borne transmission via the mechanical fixings: Numerical prediction model and experimental evaluation, Applied Acoustics 122 (2017) 88–97.

[24] S. Secchi, G. Cellai, P. Fausti, A. Santoni, N. Z. Martello, Sound transmission between rooms with curtain wall façades: A case study, Building Acoustics 22 (3-4) (2015) 193–207.

[25] A. Santoni, P. Fausti, Field measurements to analyse flanking transmission in buildings., in: Proceedings of Forum Acusticum 2014, EAA, Krakow, Poland, 2014, pp. 1–5.

[26] A. Santoni, P. Fausti, Case studies on the application of EN 12354-5 in Italy., in: Proceedings of the 42^{nd} International Congress and Exposition on Noise Control Engineering, Vol. 247, Institute of Noise Control Engineering, Innsbruck, Austria, 2013, pp. 6211–6220.

[27] E. Nilsson, A. Nilsson, Prediction and measurement of some dynamic properties of sandwich structures with honeycomb and foam cores, Journal of Sound and Vibration 251 (3) (2002) 409–430.

[28] D. Backström, A. C. Nilsson, Modelling the vibration of sandwich beams using frequency-dependent parameters, Journal of Sound and Vibration 300 (3) (2007) 589–611.

[29] A. Santoni, P. Bonfiglio, F. Mollica, P. Fausti, F. Pompoli, V. Mazzanti, Vibro-acoustic optimisation of wood plastic composite systems, Construction and Building Materials 174 (2018) 730–740.

[30] B. Van Damme, H. M. Tröbs, S. Schoenwald, Frequency dependent material properties to model the dy-namics of cross laminated timber, in: Proceedings of the International Conference on Noise and Vibration Engineering, ISMA, KU Leuven, Leuven, Belgium, 2016, pp. 1779–1786.

[31] R. Szilard, Theories and applications of plate analysis: classical numerical and engineering methods, John Wiley & Sons, Inc., Hoboken, NJ, USA, 2004.

[32] A. Nilsson, B. Liu, Vibro-acoustics, Vol. 1, Science Press, Beijing and Springer-Verlag, Berlin Heidelberg, 2015.

[33] H. Nelisse, O. Beslin, J. Nicolas, Fluid–structure coupling for an unbaffled elastic panel immersed in a diffuse field, Journal of Sound and Vibration 198 (4) (1996) 485–506.

[34] C. E. Wallace, Radiation resistance of a rectangular panel, The Journal of the Acoustical Society of America 51 (3B) (1972) 946–952.

[35] S. Ghinet, N. Atalla, Vibro-acoustic behaviour of multi-layer orthotropic panels, Canadian Acoustics 30 (3) (2002) 72–73.

[36] J. Anderson, M. Bratos-Anderson, Radiation efficiency of rectangular orthotropic plates, Acta Acustica united with Acustica 91 (1) (2005) 61–76.

[37] F. G. Leppington, E. G. Broadbent, K. H. Heron, The acoustic radiation efficiency of rectangular panels, in: Proceedings of the Royal Society of London A: Mathematical, Physical and Engineering Sciences, Vol. 382, The Royal Society, 1982, pp. 245–271.

[38] F. G. Leppington, K. H. Heron, E. G. Broadbent, S. M. Mead, Resonant and non-resonant acoustic properties of elastic panels. I. The radiation problem, in: Proceedings of the Royal Society of London A: Mathematical, Physical and Engineering Sciences, Vol. 406, The Royal Society, 1986, pp. 139–171.

[39] E. Piana, P. Milani, N. Granzotto, Simple method to determine the transmission loss of gypsum panels, in: Proceedings of the 21^{nd} International Congress on Sound and Vibration Proceedings, Vol. 21, International Institute of Acoustics and Vibration, Beijing, China, 2015.

[40] C. Hopkins, Sound insulation, 1st Edition, Butterworth-Heinemann, Oxford, UK, 2007.

[41] EN ISO 10140-5 – Acoustics: Laboratory measurement of sound insulation of building elements–Part 5: Requirements for test facilities and equipment, Standard, International Organization for Standardization, Geneva, CH (2010).

[42] N. Hashimoto, Measurement of sound radiation efficiency by the discrete calculation method, Applied Acoustics 62 (4) (2001) 429–446.

[43] A. Santoni, S. Schoenwald, B. Van Damme, P. Fausti, Determination of the elastic and stiffness characteristics of cross-laminated timber plates from flexural wave velocity measurements, Journal of Sound and Vibration 400 (2017) 387–401.

[44] T. Pritz, Frequency dependences of complex moduli and complex poisson's ratio of real solid materials, Journal of Sound and Vibration 214 (1) (1998) 83–104.

[45] M. Carfagni, M. Pierini, Determining the loss factor by the power input method (PIM), Part 1: Numerical investigation, Journal of Vibration and Acoustics 121 (3) (1999) 417–421.

[46] M. Carfagni, M. Pierini, Determining the loss factor by the power input method (PIM), Part 2: Experimental investigation with impact hammer excitation, Journal of Vibration and Acoustics 121 (3) (1999) 422–428.

[47] D. Bies, S. Hamid, In situ determination of loss and coupling loss factors by the power injection method, Journal of Sound and Vibration 70 (2) (1980) 187–204.

[48] R. Cherif, N. Atalla, Experimental investigation of the accuracy of a vibroacoustic model for sandwich-composite panels, The Journal of the Acoustical Society of America 137 (3) (2015) 1541–1550.

[49] B. C. Bloss, M. D. Rao, Estimation of frequency-averaged loss factors by the power injection and the impulse response decay methods, The Journal of the Acoustical Society of America 117 (1) (2005) 240–249.

[50] J. G. Richter, B. Zeitler, I. Sabourin, S. Schoenwald, Comparison of different methods to measure structural damping, Canadian Acoustics 39 (3) (2011) 54–55.

[51] A. Santoni, P. Bonfiglio, P. Fausti, S. Schoenwald, H.-M. Tröbs, Sound radiation efficiency measurements on cross laminated timber plates, in: Proceedings of the 45^{nd} International Congress and Exposition on Noise Control

Engineering, Institute of Noise Control Engineering, Hamburg, Germany, 2016, pp. 3697–3707.
[52] G. Squicciarini, D. Thompson, R. Corradi, The effect of different combinations of boundary conditions on the average radiation efficiency of rectangular plates, Journal of Sound and Vibration 333 (17) (2014) 3931–3948.
[53] A. Santoni, P. Bonfiglio, P. Fausti, S. Schoenwald, Predicting sound radiation efficiency and sound transmission loss of orthotropic cross-laminated timber panels, in: Proceedings of Meetings on Acoustics, Acoustics'17, Vol. 30, ASA, EAA, 2017, p. 015013.